

Supporting Information

Lele et al. 10.1073/pnas.1212327109

SI Text

Fluorescence Recovery After Photobleaching. We used a Nikon total internal reflection fluorescence (TIRF) microscope (Nikon Eclipse Ti-U) with a 25-mW 515-nm laser (Cobolt Fandango) focused in the back focal plane of a 60× TIRF objective to generate an evanescent laser field with a characteristic decay length of 100 nm. The laser was gated on and off with an electromechanical shutter (Vincent LS6). Images of motors tethered by hooks were recorded with a back-illuminated, cooled (−55 °C), electron-multiplying CCD camera (DV887ECS-BV; Andor Technology). For fluorescence recovery after photobleaching (FRAP) experiments, we photobleached with the evanescent field, using full laser power for 7 s. Analyses of images (70 frames at 0.1-s exposure) obtained during photobleaching were fitted to a model for exponential decay to reveal the extent of bleaching for every motor studied. To minimize photobleaching during image acquisition during recovery, images were taken every 20 s with 0.2-s exposures with the laser attenuated by a factor of 8. To analyze and track the motor spots in all frames, we used a centroid tracking algorithm (1) and measured motor brightness by summing over pixel intensity values within a circular mask (~450 nm diameter). Diameters were obtained (Fig. 1A) from the squared radius of gyration, i.e., the second moment of each motor brightness distribution, from the TIRF images.

Motor Intensity Measurements and z-Axis Focusing. The two cameras were not parfocal. A 350-nm latex particle (Polysciences) sitting on the coverglass surface and focused in phase contrast at the Thorlabs camera brought the focal plane for fluorescence to within ~50 nm of the surface, thus focusing the image of a tethered motor at the Andor camera. To accurately locate the particle focus along the z axis for each measurement, we custom wrote Labview programs, which enabled online particle detection and continuous tracking of the total brightness of the latex beads. The coefficient of variance in diameters of the beads was less than 2%, which allowed us to focus within ~50 nm of tethered motors for all of the different strains we studied. To correct for drift during FRAP measurements, the focus was manually adjusted to maintain the bead brightness at a constant value. In separate tests, we confirmed that such a method allowed us to maintain focus within a distance of 100 nm of the focal plane of interest (±50 nm). The laser power and camera settings were kept constant, thus ensuring identical lighting conditions for all of the motors studied. We also confirmed using 40-nm yellow beads (Polysciences) focused under TIRF illumination that the microscope point-spread function is insensitive to variations in focus on the order of ±50 nm.

Model for Adaptation. A wild-type switching cell with a fixed CheY-P level is assumed to be in a steady state with regard to the total number of FliM molecules (N_{ss}) within the motor. As observed experimentally, this N_{ss} consists of two populations, the exchanging population C_{ss} that continuously exchanges on the timescale of observations and the nonexchanging population N_{ne} . Thus, as noted in the main text, the equation describing the time rate of change of the number of FliM molecules in a motor, N , is

$$\frac{dN}{dt} = \frac{dC}{dt} = k_{on}UB - k_{off}C, \quad [S1]$$

where U is the number of unbound FliM molecules in the cell, and B is the number of vacant sites.

Addition of a strong attractant to a *cheR cheB* cell rotating exclusively clockwise (CW) disturbs the steady state by reducing CheY-P to a very low fixed level, such that the motor switches to exclusively counterclockwise (CCW) rotation. During the CCW rotation, the rotor conformation causes the FliM molecules already present in the motor ($N_{ss} = 34$) to bind tightly, increasing the nonexchanging population at $t = 0$. For simplification, we assume $N_{ne} = N_{ne}^{CCW}$, i.e., that all 34 FliM become strongly attached. Because under strong attractant, the CW_{bias} of *cheR cheB* cells remains 0, the rotor presumably does not change conformation after $t = 0$. Hence we assume that N_{ne} remains constant for the rest of the time ($N_{ne} = N_{ne}^{CCW}$). However, the FliM ring is not at steady state; the numbers of vacant sites, $B(t)$, and of exchanging FliM molecules, $C(t)$, vary over time until a new steady state is reached. At the new steady state, the values of $C(t \rightarrow \infty)$ and $B(t \rightarrow \infty)$ will satisfy Eqs. 2 and 4 (main text). Eq. 1 can be solved, and we obtain the total FliM population variation,

$$N(t) = \frac{1}{2} (M - N_{ne}^{CCW} - (M - N_{ne}^{CCW} - 2(N_{ss} - N_{ne}^{CCW}))e^{-2k_{off}t}) + N_{ne}^{CCW}, \quad [S2]$$

which is shown in Fig. 3B (solid curve) after normalization by N_{ss}^{CCW} .

Whereas this analysis addresses the case of a strong attractant, where CW bias does not recover even though the FliM content changes, the analysis can be extended for weak attractants by assuming that the nonexchanging population N_{ne} varies with CW_{bias} .

Reversing the arguments for a predominantly CCW motor treated with a strong repellent, with the initial condition $C(0)/N_{ss} = (N_{ss} - N_{ne}^{CW})/N_{ss}$, yields the equation

$$N(t) = \frac{1}{2} (M - N_{ne}^{CW} - (M - N_{ne}^{CW} - 2(N_{ss} - N_{ne}^{CW}))e^{-2k_{off}t}) + N_{ne}^{CW}, \quad [S3]$$

which is shown in Fig. 3B (shaded curve) after normalization by N_{ss}^{CW} .

Correction for Bleaching of Unbound FliM Molecules. Consider that all of the FliM molecules are fluorescent. Then Eqs. 1–4 can be rewritten with the only change being the use of variables N^f , C^f , and U^f , where the superscript f refers to fluorescently active molecules (N_{ss}^f is the initial motor brightness or I_{pre}). The steady state can be disturbed by photobleaching the motor. Because the bleached exchanging population C continuously exchanges with other fluorescent molecules in the cell, the motor brightness, $I(t)$, will recover over long times to a fraction of the initial intensity

I_{pre} , such that under ideal conditions, $\frac{I(t \rightarrow \infty)}{I_{pre}} = \frac{C_{ss}^f}{N_{ss}^f}$. However, the application of a TIRF photobleaching pulse with full laser power on our setup leads to a partial photobleaching of the unbound fluorescent population, U^f , to a lower value U_c^f . As explained in the next section, we measure the ratio of U_c^f/U^f , experimentally. The governing equation for the recovery in fluorescence has the same form as Eq. 1,

$$\frac{dC^f}{dt} = k_{on}U_c^fB - k_{off}C^f, \quad [S4]$$

subject to the initial conditions $C_{t=0}^f = \alpha C_{ss}^f$, yielding the solution:

$$C^f(t) = \frac{U_c^f C_{ss}^f}{U^f} (1 - e^{-k_{off}t}) + \alpha C_{ss}^f e^{-k_{off}t}, \quad [S5]$$

where $C_{ss}(t) = \frac{k_{on}U^f B_{ss}}{k_{off}}$, and α denotes the extent of bleaching, which we measure experimentally for every motor studied. The visible population in our experiments is $I(t) = C^f(t) + \alpha N_{ne}^f$.

Then the normalized intensities are

$$\frac{\hat{I}(t) - \hat{I}(0)}{I_{pre} - I(0)} = \frac{C_{ss}^f}{N_{ss}^f (1 - \alpha)} (1 - e^{-k_{off}t}) \left(1 - \alpha \frac{U^f}{U_c^f}\right), \quad [S6]$$

where

$$\hat{I}(t) = \frac{U^f}{U_c^f} I(t).$$

This expression reduces to the familiar FRAP data-fit expression $\frac{C_{ss}^f}{N_{ss}^f} (1 - e^{-k_{off}t})$ at very low values of α . Importantly, photobleaching of the unbound FliM population does not affect measurements of rates as can be seen from the above equation, consistent with previous modeling of TIRF-based FRAP (2)

1. Crocker JC, Grier DG (1996) Methods of digital video microscopy for colloidal studies. *J Colloid Interface Sci* 179:298–310.
2. Fukuoka H, Inoue Y, Terasawa S, Takahashi H, Ishijima A (2010) Exchange of rotor components in functioning bacterial flagellar motor. *Biochem Biophys Res Commun* 394(1):130–135.
3. Delalez NJ, et al. (2010) Signal-dependent turnover of the bacterial flagellar switch protein FliM. *Proc Natl Acad Sci USA* 107(25):11347–11351.

Demonstration That TIRF Is Appropriate for Bleaching. It has been suggested that evanescent fields used here and by Fukuoka and coworkers (2) might not be suitable for studies of FRAP, because long-term bleaching [generated by a 7-s exposure, as opposed to the 0.3-s exposure used by Delalez et al. (3)] might lead to a drastic reduction in FliM-eYFP contained in the inner membrane or in the cytoplasm. If so, nonrecovery after photobleaching might be due to a paucity of FliM-eYFP. To check for this possibility, we compared total cell fluorescence measured by epifluorescence immediately before and after bleaching with the evanescent field. Although we completely bleached the tethered motor, 70% of the fluorescence seen in epifluorescence remained. Fig. S2 shows one such cell.

CW_{bias} and Speed of FliG Mutant Motors. Previous work showed that a 3-amino-acid deletion at positions 169–171 in the FliG sequence in *Salmonella typhimurium* leads to an extreme CW bias of the flagellar motor, without affecting its other properties (4, 5). We introduced this mutation in *Escherichia coli* and observed 100% CW bias with rotational speeds similar to those of wild-type motors when rotating CW. This was true even when the recipient strain was deleted for *cheY*, a deletion that normally promotes 100% CCW rotation. Introducing this mutation in the CCW strain yielded exclusively CW motors. The average speed for the CW strain was 5.3 ± 0.6 Hz compared with an average speed of 6.2 ± 0.51 Hz for the CCW strain with wild-type *fliG*.

4. Togashi F, Yamaguchi S, Kihara M, Aizawa SI, Macnab RM (1997) An extreme clockwise switch bias mutation in *fliG* of *Salmonella typhimurium* and its suppression by slow-motile mutations in *motA* and *motB*. *J Bacteriol* 179(9):2994–3003.
5. Minamino T, et al. (2011) Structural insight into the rotational switching mechanism of the bacterial flagellar motor. *PLoS Biol* 9(5):e1000616.

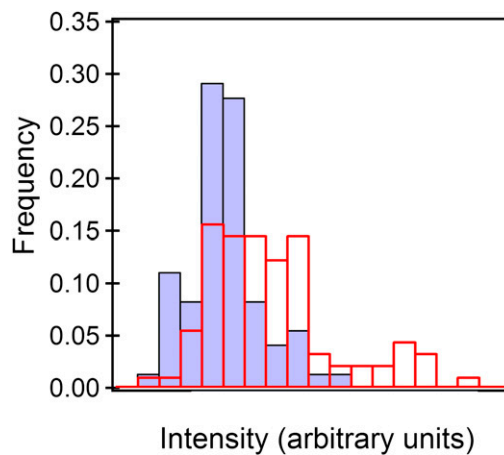


Fig. S1. Histograms for motor FliM distributions: CW (blue, $n = 72$ motors) and CCW (red, $n = 89$ motors).

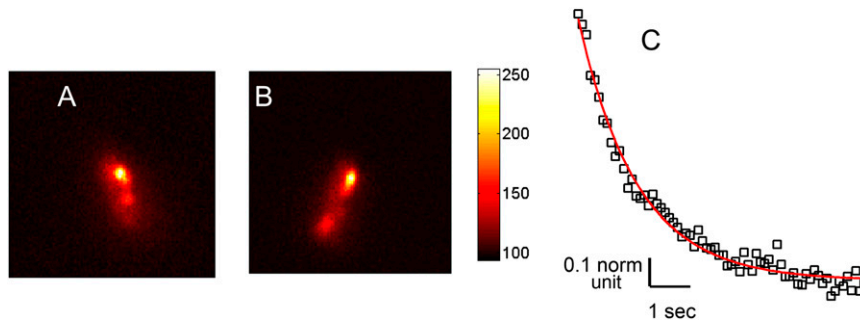


Fig. S2. (A) Epifluorescence image of a tethered cell before bleaching. (B) Epifluorescence image of the same cell after a 7-s exposure to the evanescent field. (C) Normalized motor intensities during the 7-s exposure with the exponential decay model (red curve).

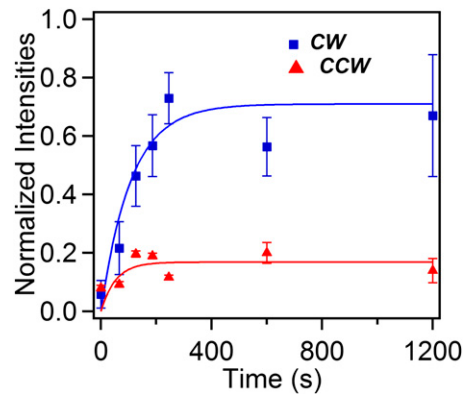


Fig. S3. Recovery over long times in average fluorescence intensities in CW and CCW strains after photobleaching.

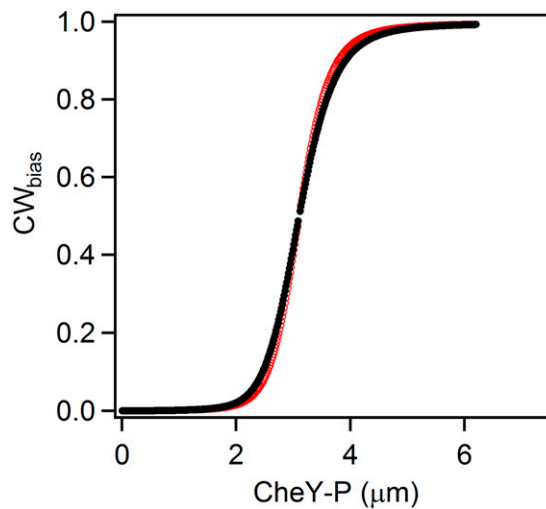


Fig. S4. Predictions of CW_{bias} from the conformational spread model (1), for different ring sizes. Red curve, $n = 42$, and black curve, $n = 34$, with $E_a = 0.65 k_B T$, $E_j = 4.13 k_B T$. The curves almost coincide, suggesting that no adaptation will occur because the CW_{bias} at any given CheY-P level is similar for different ring sizes. Similar coinciding curves are obtained with the MWC model (2).

1. Duke TA, Le Novère N, Bray D (2001) Conformational spread in a ring of proteins: A stochastic approach to allostery. *J Mol Biol* 308(3):541–553.
2. Alon U, et al. (1998) Response regulator output in bacterial chemotaxis. *EMBO J* 17(15):4238–4248.